Research Article

Structural, thermal and electrical properties of composites electrolytes (1−x) CsH_2PO_4/x ZrO_2 ($0 \le x \le 0.4$) for fuel cell with advanced electrode

Deshraj Singh[1] · Pawan Kumar[2] · Jitendra Singh[1] · Dharm Veer[2] · Aravind Kumar[3] · Ram S. Katiyar[4]

Received: 6 August 2020 / Accepted: 28 December 2020 / Published online: 8 January 2021

Abstract
Composites proton conducting material based on cesium dihydrogen phosphate (CDP) doped with zirconium oxide (1−x) CsH_2PO_4/x ZrO_2 were synthesized with different concentration having in the range such as x = 0.1, 0.2, 0.3 and 0.4 by ball milling method. The prepared solid acid composites were dried at 150 °C for 6 h. Structural and thermal characterization of solid acid composite proton electrolytes were carried out by X-ray diffractometer, Fourier transform infrared spectroscopy, and Raman spectroscopy respectively. Phase transition of the prepared materials was carried out by using differential scanning calorimetry and conductivity was measured by LC Impedance meter in the range 1 Hz to 400 kHz. The ionic conductivity of ZrO_2 doped CsH_2PO_4 (CDP) was increased up to 1.3×10^{-2} S cm^{-1} at the 280 °C under environment atmospheric humidification which showed high stability as compared to pure CsH_2PO_4 (CDP). This obtaining result would be useful for establishing and design the next generation fuel cell.

Keywords CsH_2PO_4 · Electrolyte · Conductivity · Fuel cell

1 Introduction

Fuel cells are an electrochemical cell that converts chemical energy into electrical energy through electrochemical reactions. Fuel cells are a unique array for a potential application, and similar to batteries but do not need to recharge. The basic component of a fuel cell is anode, cathode, and electrolytes. The core source of a fuel cell is hydrogen which helps to transfer ions from cathode to anode. Solid electrolytes are exhibit high ionic conductivity, low activation energy, good mechanical properties, and are found to be promising materials for solid-state batteries, fuel cells, sensors, memory cells, solid-state batteries, etc. [1, 2]. There are two reasons for the high ionic conductivity of these superionic materials, one is the presence of a large number of defects and vacancies in the lattice at room temperature and the second is the low coordination number of the mobile ions [3–5]. There are several new materials for efficient proton conductivity, among them cesium dihydrogen phosphate (CDP), showing a superprotonic phase transition at 230 °C [6, 7]. The high-temperature conductivity is increased several orders of the magnitude at the transition temperature from 223 °C to 233 °C, the ionic conductivity increases from 8.5×10^{-6} S cm^{-1} to 1.8×10^{-2} S cm^{-1} [8] and CDP with 80 wt% represent a high ionic conductivity of 1.1×10^{-2} S cm^{-1}at 259 °C [9]. At the transition temperature CDP changed from the monoclinic phase to the tetragonal (cubic) phase, this changed increase ionic conductivity followed by the Grotthuss mechanism [10]. Above 230 °C CDP chemical transformation decomposed as

$$2CsH_2PO_4 \rightarrow Cs_2H_2P_2O_7 + H_2O$$

✉ Pawan Kumar, pksoniyal13@gmail.com | [1]Department of Physics K.G.K. College, Moradabad, M.J.P. Rohilkhand University, Bareilly 243006, India. [2]Department of Physics, Gurukul Kangri University, Haridwar 249404, India. [3]Department of Physics, Kalindi College, Delhi University, Delhi, India. [4]Department of Physics, University of Puerto Rico, San Juan, PR 00931, USA.

So, the superprotonic phase of CDP is unstable because of its dehydration under normal conditions [11]. It is thermally stable in an atmosphere containing more than 30 mol% H_2O, which is not favorable for fuel cell electrolytes [12]. We need some modification by using heterogeneous doping of highly inert oxide ZrO_2, SiO_2, TiO_2, Al_2O_3 and rare-earth phosphate with CDP produces a supercooling effect on the conductivity by ball milling method. Ball milling is a method for enhancing the material reactivity and uniformity of distribution of elements which is economically and environmentally sustainable. The ability of thermal and mechanical stability improves by such type of doping above the transition temperature [13–16]. An enhancement of the ionic conductivity was detected for CsH_2PO_4–$SrZrO_3$ [17] and CsH_2PO_4-SiO_2 [18, 19] composite electrolytes. Ponomareva et al. [20] observed that the conductivity of CDP at low temperatures was improving several orders by small amount doping of SiO_2. Kikuchi et al. [21] observed $CsH_5(PO_4)_2/SiP_2O_7$ exhibit higher conductivity 500 mS cm^{-1} than pure $CsH_5(PO_4)_2$ 160 mS cm^{-1}.

In the present work, we will observe the transport, thermal properties and ionic conductivity of the composite electrolytes 0.9CDP-0.1ZrO_2, 0.8CDP-0.2ZrO_2, 0.7CDP-0.3ZrO_2, and 0.6CDP-0.4ZrO_2 at different temperature.

2 Experimental

Cesium dihydrogen phosphate (CDP), was synthesized by slow evaporation under ambient conditions from an aqueous solution of Cs_2CO_3 (99%, Alfa Aesar) and phosphoric acid H_3PO_4 (≥ 85 wt. % in H_2O, Alfa Aesar) according to the following reaction [22]:

$$Cs_2CO_3 + 2H_3PO_4 \rightarrow 2CsH_2PO_4 + CO_2 + H_2O$$

Dissolve 25 gm Cs_2CO_3 in 200 ml distilled water, 15 ml 98% H_3PO_4 previously dissolve in 200 ml distilled water was added to the solution prepared above dropwise, using a burette. The total volume of the solution becomes 400 ml. The solution was stirred for 6 h. Thereafter, the obtained solution was heated in an oven at 150 °C until it turns in a hard-solid amorphous bottom layer. The solid layer was washed with methanol and vacuum-filtered then dried at 120 °C for 2 h to remove the residual water and grinded to produce the powder of CDP [7]. X-ray diffraction (XRD) pattern of initial powders and mixtures were recorded with Proto Axrd Benchtop ($K\alpha_{1,2}$ or K_β wavelength, the energy resolution of 200 eV FWHM, 640 channel high-speed detector). Finally, the (1−x) CsH_2PO_4/x ZrO_2 where x = (0.0–0.4) composites synthesized. ZrO_2 particles that were purchased from Alfa Aesar and added into dry crystalline/amorphous precipitate produced in the above method according to their weight percent. The constituents were mixed in an agate mortar for 4 h and a homogeneous powder mixture was prepared. The powder was pressed in the form of a pallet by hydraulic pellet pressing at 7 tons for 20 min. The diameter and thickness of the pellet were 10.0 mm and 3 mm, respectively. The pellets were calcined at 80 °C for 2 h. Silver was used for making electrodes on the surface of pellets by advanced vacuum coating unit (Hind High Vacuum-12A4D). The conductivity was measured by LC Impedance Meter (Hikoki 3532–50) in the frequency range 1 Hz to 400 kHz at the temperature range from room temperature to 300 °C. The ionic conductivity value was calculated from the resistance value of R. Temperature dependences of the conductivity plotted in Arrhenius plots form by the following equation,

$$\sigma(\mathrm{S/cm}) = \mathrm{L(cm)/A}\left(\mathrm{cm}^2\right) \mathrm{R}(\Omega)$$

where R is the resistance, L is the thickness of the electrolyte pellet and A is the area of the electrolyte pellet.

Differential scanning calorimetry (DSC) data were obtained by the (DSC-60) Unit (Shimadzu, Japan) system in the temperature range of 20 °C to 400 °C at a heating rate of 5 °C/min under 50 ml/min nitrogen flow. Phase transitions of the materials were measured by the DSC. Thermogravimetric analysis (TGA) and Differential thermal analysis (DTA) data were obtained with a Perkins Elemer 4000 system. Fourier Transform Infrared Spectroscopy (FTIR) was used to identify the number of components and the presence of any functional group in the material. FTIR data was collected by FTIR- 8400S Unit (Schimadzu, Japan). RAMAN data was collected by micro –Raman system (Horiba-Jobin T64000) equipped with an Ar laser in the range 100–1000 cm^{-1}.

3 Results and discussion

3.1 X-ray diffraction (XRD)

The X-ray diffraction (XRD) patterns of the CDP and combination of CDP with ZrO_2 in the range 2θ = 20°–60° are plotted in Fig. 1.

The XRD patterns of the CDP and CDP/ZrO_2 electrolyte composites were measured in the powdered form under the atmospheric condition, after heat treatment of 100 °C for 2 h. The sharp and well resolved diffraction peaks obtained at 2θ values of 23.6°, 29.0°, 36.8°, 38.1° and 48.2° of CDP correspond to (011), (111), (220), (2 21), and (311) planes respectively. The experimentally measured diffraction pattern for CDP is the same as standard data from JCPDS of CDP and ZrO_2 card No. 84–0122 and 37–1484 respectively [23, 24]. CDP powder showed a monoclinic

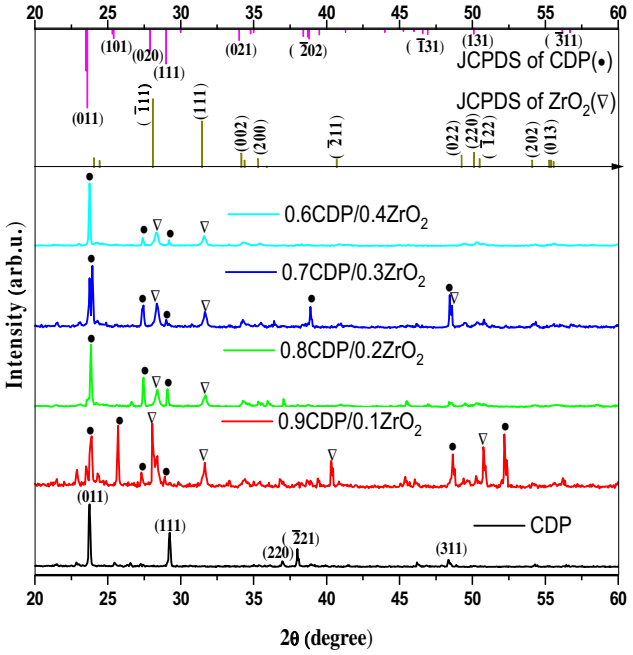

Fig. 1 XRD patterns of powdered CsH_2PO_4/ZrO_2 composites. CsH_2PO_4 and monoclinic ZrO_2 are indexed according to JCPDS card No. 84–0122 and 37–1484 respectively

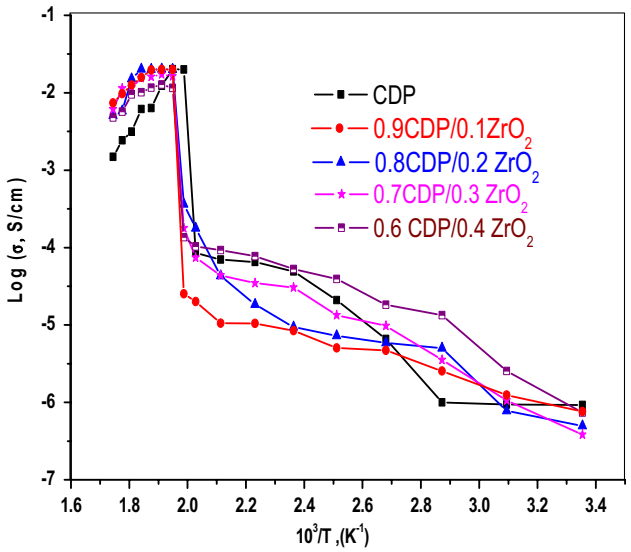

Fig. 2 Arrhenius plots of Temperature dependence conductivity for CDP and its Composites $0.9CDP/0.1ZrO_2$,$0.8CDP/0.2ZrO_2$, $0.7CDP/0.3ZrO_2$ and $0.6CDP/0.4ZrO_2$

phase with space group $P2_1/m$ and ZrO_2 powder also monoclinic phase at room temperature. All peaks of the composites are the same as observed for CDP and ZrO_2.

3.2 Conductivity

Temperature dependence conductivity of composites (1–x) CDP-xZrO_2 where $x \leq 0.4$ (CDP/ZrO_2 ratio of 0.9/0.1, 0.8/0.2, 0.7/0.3, and 0.6/0.4) were studied. The arrehenius plots at various temperatures are shown in Fig. 2**.**

The conductivity of CDP increases by three orders of magnitude at the transition temperature. The ionic conductivity of CDP was found out 10^{-6}S cm^{-1} at 150 °C which is increased 10^{-2}S cm^{-1}at 230 °C with an activation energy ≈ 0.4 eV. The Arrhenius plot of conductivity jumped with an activation energy of 0.88 eV at a higher temperature which was 1.28 eV below the 180 °C [25, 26]. At cold sintering process, ionic conductivity of CDP reaches 2.30×10^{-4} S cm^{-1} at 200 °C because it is highly dissolving material with water [2]. The presence of ZrO_2 increases the stability of solid acid composites due to the imperfect interconnections between the solid acid and ZrO_2 [27]. Above 250 °C CDP dehydrates so conductivity starts to decreases for removing this problem introduced ZrO_2. In this work, the conductivity of CDP reached a maximum of 2.0×10^{-2} S cm^{-1} at the 240 °C and 6.4×10^{-3} S cm^{-1} at the 260 °C. Only the temperature between 230 °C (transition temperature) to 250 °C (decomposition temperature) pure CDP exhibited high conductivity, after introducing ZrO_2 in CDP this range increase from 230 to 300 °C. The conductivity of $0.7CDP/0.3ZrO_2$ and $0.6CDP/0.4ZrO_2$ was observed 1.14×10^{-2} S cm^{-1} at the temperature of 290 °C and 4.76×10^{-3} S cm^{-1} at the temperature of 300 °C, respectively which shows the stability increases and conductivity slightly decreases with increasing of x. Introducing of ZrO_2 was a good increment to stopping decomposition. After 280 °C the conductivity of CDP/ZrO_2 mixture starts decreases slowly as temperature crossed 300 °C, it decreases fast. Conductivity measured for pure CDP and CDP/ZrO2 at the temperature 25 °C, 50 °C, 75 °C, 100 °C, 125 °C, 150 °C, 175 °C, 200 °C, 220 °C, 230 °C, 240 °C, 250 °C, 260 °C, 270 °C, 280 °C, 290 °C and 300 °C. Leal et al. [28], Anfimova et al. [29], Ponomerva et al. [30] reported a result for enhancing the conductivity and stability of other composites electrolytes.

If the container of pellet confined in a high pressure, the protonic conductivity of $0.9CDP/0.1ZrO_2$ and $0.8CDP/0.2ZrO_2$ was 1.8×10^{-2} S cm^{-1} for 2000 min and 1.3×10^{-2} S cm^{-1} for 2200 min, respectively as soon in Fig. 3.

3.3 Differential scanning calorimetry (DSC)

Typical thermal analyses for CDP and CDP with ZrO2 at different composition ratios with the constant heating rate (5 °C/min) are presented in Fig. 4.

The DSC data for the CDP shows endothermic peaks at 150 °C, 230 °C, 270 °C, and 295 °C which are most likely related to the protonic phase transition. The transition at

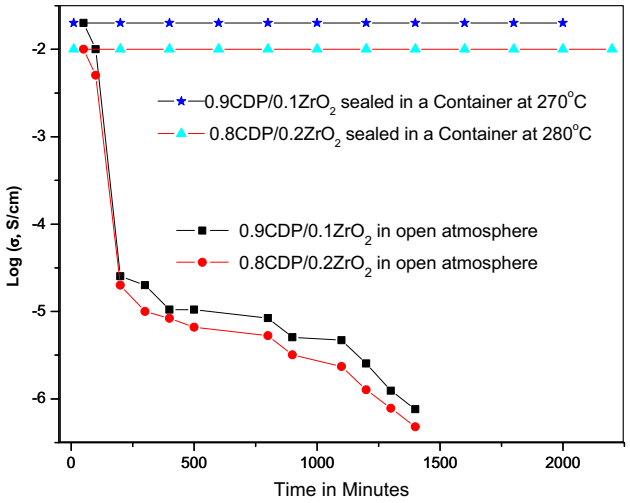

Fig. 3 Time dependence of the conductivity for the CDP/ZrO_2 in open atmosphere and hermetically sealed in a container

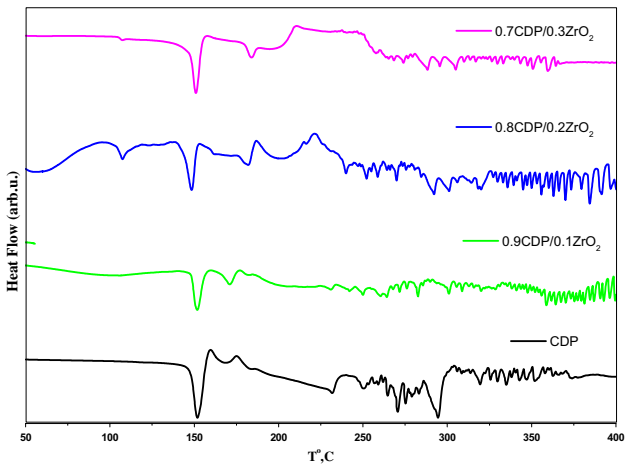

Fig. 4 Differential Scanning Calorimetry (DSC) curves for CDP and its composites heating rate 5 °C/min

150 °C is quasi-irreversible because hydrogen-bonded in CDP are ferroelectrics, so at the 150 °C peak is due to the presence of a small amount of $CsH_5(PO_4)_2$ and ferroelectric transition take place which is quasi-irreversible [31]. Transition at 230 °C occurs due to the formation of monoclinic transition to cubic (superprotonic) transition and 270 °C due to dehydration of composites electrolytes [32] as shown in Fig. 4. 295 °C transition occurs due to the formation of polymers dehydration of the phosphate ions. The endothermic peaks were observed in composites 0.9CDP-0.1ZrO_2, 0.8CDP-0.2ZrO_2, and 0.7CDP-0.3ZrO_2 at the temperature of 264 °C and 335 °C, 270 °C and 347 °C, 288 °C and 359 °C respectively which is more stable then pure CDP. The enthalpy of phase transition decreases more rapidly on increasing the value of x in (1−x) CDP/xZrO_2 (where x = 0.1 to 0.4), which is indicating that the thermal stability of the CDP enhanced [18]. The CDP with different compositions of ZrO_2 shows distinctive peaks between 150 °C and 400 °C due to the dehydration of present additives.

3.4 Thermogravimetric analysis (TGA) and differential thermal analysis (DTA)

A plot of the TGA and DTA investigated at a different temperature from a powder of CDP and CDP/ZrO_2 composites is shown in Fig. 5A and Fig. 5B. The weight loss for CDP/ZrO_2 is less as compared with the pure CDP, So the weight loss decreases as the value of x increases. The important decrease of the weight was obtained after 200 °C, which indicated dehydration of CDP as in Fig. 5A. Thus, the conductivity is directly influenced by dehydration of CDP and its composites.

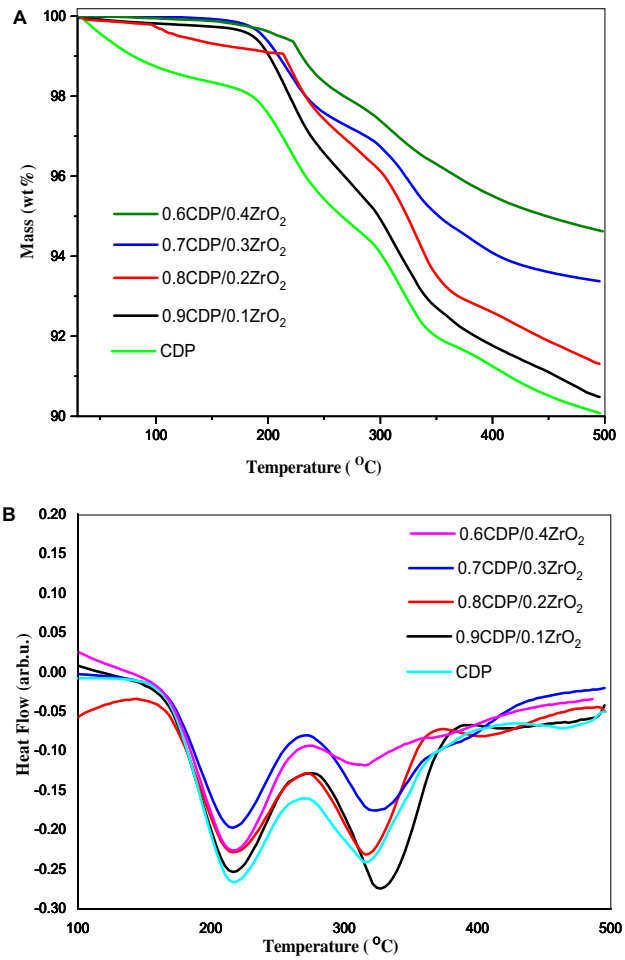

Fig. 5 TGA **(a)** and DTA **(b)** of powder CDP and composite electrolytes CDP/ZrO2 with dry air flow 60 ml/minute with a heating rate 5 °C/minute in the temperature range 30 °C —500 °C

As well as the value of x increases, the peak of DTA is shifted towards the higher temperature which indicates the mixing of ZrO_2 increases the stability of CDP as in TGA data. The DTA curve of pure CDP and its composites in Fig. 5B showed two endothermic peaks at the temperature near about 230 °C and 320 °C. The endothermic peak arises due to phase transition from the monoclinic phase to the cubic phase and the second one endothermic peak at the temperature of 320 °C is due to completely dehydration of the liquid phase as a sharp mass loss.

3.5 Fourier transform infrared spectroscopy (FTIR)

The FTIR spectra of the CDP, binary mixtures of CDP with ZrO_2, and the intense band of the group Zr-OH, Zr-O-Zr, and Zr-O are shown in the Fig. 6**.**

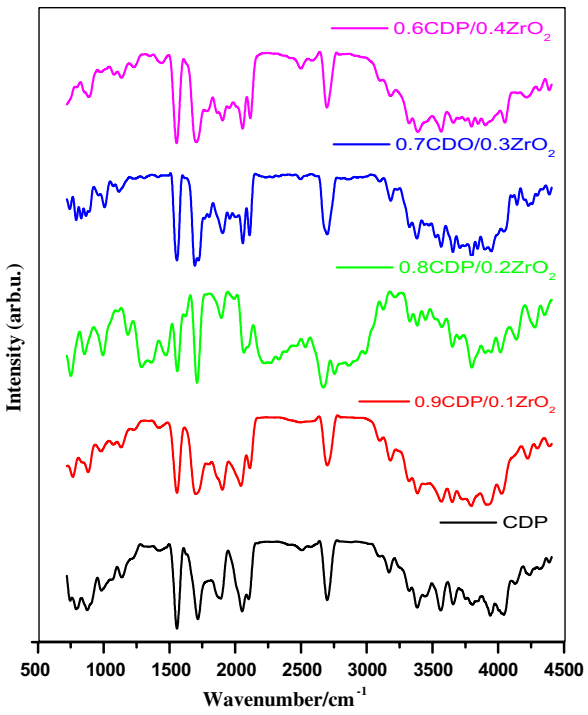

Fig. 6 O–H modes, Stretching P–O, bending P–OH, O–P–O modes and Cs–O modes in FT-IR Spectra of CDP and comparison its composites 0.9CDP/0.1ZrO_2, 0.8CDP/0.2ZrO_2, 0.7CDP/0.3ZrO_2 and 0.6CDP/0.4ZrO_2 in the range of 400 to 4000 cm^{-1}

To determine the presence of hydrogen bonds and PO_4^{3-} anions in the present composite electrolytes, infrared transmittance spectra of the material was taken in the range of 400 cm^{-1} to 4000 cm^{-1}. There are many well-separated regions in the infrared spectrum in high frequency (OH) modes 3600 cm^{-1} to 1300 cm^{-1}, Stretching P–O, and bending P–OH modes 1300 cm^{-1} to 800 cm^{-1} and O–P–O modes and Cs-O belongs to 800 cm^{-1} to 400 cm^{-1}[33]. The material monoclinic ZrO_2 sharp band is appearing at 746 cm^{-1}. The proton-conducting behavior of the electrolytes exists with the type of hydrogen bonds [34]. O–H band separated into ν (OH), δ (OH), γ (OH) due to Fermi resonance overtones of the deformation modes appear as the ABC structure [35, 36]. In our study, the peaks were observed at 2760 cm^{-1}, 2332 cm^{-1}, and 1700 cm^{-1} which are indicated to the O–H stretching bands. The strong bands δ(PO–H) measured at 1216 cm^{-1}, ν_3PO_4 asymmetric and symmetric stretching observed at 1085 cm^{-1} and 954 cm^{-1} respectively. The weak bands δ(PO–H) in-plane and γ(PO–H) out of the plane are also observed at 1104 cm^{-1} and 1214 cm^{-1} respectively. The Cs–OH band is arising at 531 cm^{-1} regions. Similar symmetry was also measured for other composite electrolytes. The well-separated peaks of CDP powder are shown in Table 1.

3.6 Raman spectra

Raman spectra of CDP versus temperature between the range of room temperature to − 191 °C and frequency range 100 cm^{-1} to 1000 cm^{-1} are given in Fig. 7.

Similar spectra at low temperatures up to room temperature have been discussed [11, 35], which shows the same result as our work. In the CDP, the bands are less visible due to OH− stretching. The spectrum of P–O–P bridges appears at 620 cm^{-1}. There is no large effect by temperature in the range of room temperature to − 191 °C on Raman Spectra. All the bands well defined in the spectrum of the superionic phase in CDP. The bands arising due to internal vibration of $H_2PO_4^-$ ions, is likewise appeared by the low-frequency spectra.

Table 1 Functional groups which are present in CDP

Material	Reference	Wavelength (cm^{-1})					
		Cs–O Bond	O–P–O Stretching		O–H Stretching (High Frequency)		
			Symmetric	Asymmetric			
CDP	Our paper	557	808	1085	1700	2332	2760
CDP	[25]	502	941	1070	1710	2310	2710

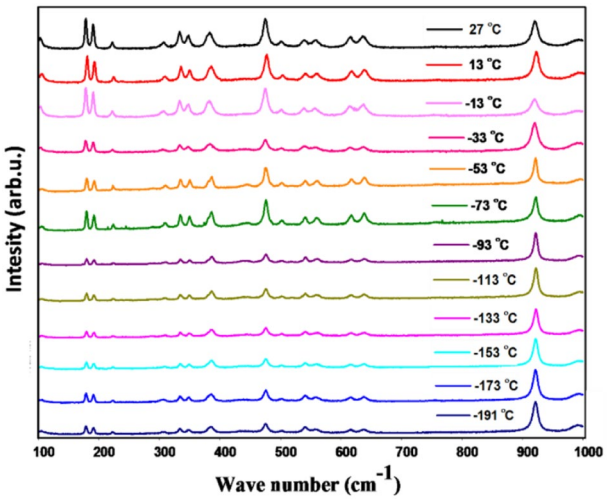

Fig. 7 Raman spectra of Cesium dihydrogen phosphate at different temperature. Phosphate ions giving rise to bands at 620 cm^{-1} (P–O–P bridge stretching)

4 Conclusions

The structural, thermal, and proton conductivity behavior of (1−x) CsH_2PO_4/x ZrO_2 ($0 \le x \le 0.4$) composites electrolytes for the fuel cell. Based on an evaluation of the literature and our recent conductivity measurements, CDP undergoes a superprotonic transition at 230 °C. A three order of magnitude ionic conductivity increases in the unmixed sample at the transition temperature. The CDP was dehydrated up to 250 °C. We were observed that CDP with low additives of ZrO_2 (contents $x = 0.1$ and 0.2) was good agreement with ionic conductivity and stability. CDP and ZrO_2 perform between the temperatures range from 230 °C to 280 °C which is a good increment. The highest conductivity of confined electrolytes 0.9CDP/0.1ZrO_2 and 0.8CDP/0.2ZrO_2 were observed 1.8×10^{-2} S cm^{-1} for 2000 min and 1.3×10^{-2} S cm^{-1} for 2200 min, respectively. The intensity was decreasing in Raman spectroscopy as well as temperature decreases. The high ionic conductivity and thermal stability of these composites make them attractive for use in different chemical devices and fuel cells.

Acknowledgements The authors are thankful to Department of Physics K.G.K. College, Moradabad, M.J.P Rohilkhand University Bareilly, India, University of Puerto Rico, Rio Piedra Campus SPECLAB, San Juan, USA, for providing me the Raman spectra facilities. The authors also thankful to Material Science Research Lab, Department of Physics, Gurukul Kangri University Haridwar (India) to provide necessary facilities.

Compliance with ethical standards

Conflict of interest The authors declare that they have no conflict of interest.

References

1. Colomban P (1992) Proton conductors solid membranes, and gels-materials and devices. Cambridge University Press 5(9):683–685
2. Nakaya H, Iwasaki M, de Beauvoir TH, Randall CA (2019) Applying cold sintering process to a proton electrolyte material: CsH_2PO_4. J Eur Ceram Soc 39:396–401. https://doi.org/10.1016/j.jeurceramsoc.2018.09.001
3. Yoshimi S, Matsui T, Kikuchi R, Eguchi K (2008) Temperature and humidity dependence of the electrode polarization in intermediate-temperature fuel cells employing CsH_2PO_4/SiP_2O_7-based composite electrolytes. J Power Sources 179(2):497–503. https://doi.org/10.1016/j.jpowsour.2008.01.003
4. He X, Zhu Y, Mo Y (2017) Origin of fast ion diffusion in superionic conductors. Nat Commun 8:1–7. https://doi.org/10.1038/ncomms15893
5. Reddy SN, Chary AS, Reddy CG, Rao MVM (2004) Effect of alumina on dc ionic conductivity of barium nitrate solid electrolyte. Mater Lett 58:2949–2952. https://doi.org/10.1016/j.matlet.2004.03.040
6. Baranov AI, Merinov BV, Tregubchenko AV, Khiznichenko VP, Shuvalov LA, Schagina NM (1989) Fast proton transport in crystals with dynamically disordered hydrogen bond network. Solid State Ionics 36:279–282. https://doi.org/10.1016/0167-2738(89)90191-4
7. Aili D, Gao Y, Han J, Li Q (2017) Acid-base chemistry and proton conductivity of $CsHSO_4$, CsH_2PO_4 and their mixtures with N-heterocycles. Solid State Ionics 306:13–19. https://doi.org/10.1016/j.ssi.2017.03.012
8. Haile SM, Chisholm CRI, Sasaki K, Boysen DA, Uda T (2007) Solid acid proton conductors: From laboratory curiosities to fuel cell electrolytes. Faraday Discuss 134:17–39. https://doi.org/10.1039/b604311a
9. Qing G, Kikuchi R, Takagaki A, Sugawara T, Oyama ST (2015) CsH_2PO_4/epoxy composite electrolytes for intermediate temperature fuel cells. Electrochim Acta 169:219–226. https://doi.org/10.1016/j.electacta.2015.04.089
10. Ortiz E, Pineres I, Leon C (2016) On the low- to high proton-conducting transformation of a $CsHSO_4$–CsH_2PO_4 solid solution and its parents. J Therm Anal Calorim 126:407–419. https://doi.org/10.1007/s10973-016-5474-y

11. Nikiforov AV, Berg RW, Bjerrum NJ (2018) Vapor pressure and specific electrical conductivity in the solid and molten H_2O-CsH_2PO_4-$CsPO_3$ system: a novel electrolyte for water electrolysis at ~ 225–400 °C. Ionics (Kiel) 24:2761–2782. https://doi.org/10.1007/s11581-017-2420-3
12. Ponomareva VG, Shutova ES (2014) New medium-temperature proton electrolytes based on CsH_2PO_4 and silicophosphate matrices. Inorg Mater 50(10):1050–1055. https://doi.org/10.1134/S0020168514100124
13. Baranov AI, Grebenev VV, Khodan AN, Dolbinina VV, Efremova EP (2005) Optimization of superprotonic acid salts for fuel cell applications. Solid State Ionics 176:2871
14. Matsui T, Kukino T, Kikuchi R, Eguchi K (2005) an intermediate temperature proton-conducting electrolyte based on a CsH_2PO_4 /SiP_2O_7 composite. Electrochem Solid State Lett 8:256–258. https://doi.org/10.1149/1.1883906
15. Yaroslavtsev AB (2005) Modification of solid-state proton conductors. Solid State Ionics 176(39–40):2935–2940. https://doi.org/10.1016/j.ssi.2005.09.025
16. Matsui T, Muroyama H, Kikuchi R, Eguchi K (2010) Development of novel proton conductors consisting of solid acid/pyrophosphate composite for intermediate-temperature fuel cells. J Jpn Petrol Inst 53:1–11. https://doi.org/10.1627/jpi.53.1
17. Lavrova GV, Shutova ES, Ponomareva VG, Dunyushkina LA (2013) Proton conductivity and interphase interaction in CsH_2PO_4-$SrZrO_3$ composites. Russ J Electrochem 49:718–724. https://doi.org/10.1134/S1023193513070094
18. Ponomareva VG, Shutova ES (2007) High-temperature behavior of CsH_2PO_4 and CsH_2PO_4–SiO_2 composites. Solid State Ionics 178:729–734. https://doi.org/10.1016/j.ssi.2007.02.035
19. Otomo J, Ishigooka T, Kitano T, Takahashi H, Nagamoto H (2008) Phase transition and proton transport characteristics in CsH_2PO_4/SiO_2 composites. Electrochim Acta 53:8186–8195. https://doi.org/10.1016/j.electacta.2008.06.018
20. Ponomareva VG, Uvarov NF, Lavora GV, Hairetdinov EF (1996) Composite protonic solid electrolytes in the $CsHSO_4$/SiO_2 system. Solid State Ionics 90:161–165
21. Kikuchi R, Ogawa A, Matsuoka T, Takagaki A, Sugawara T, Oyama S (2016) Interfacial conduction mechanism of cesium dihydrogen phosphate. Solid State Ionics 285:160
22. Mohammad N, Mohamad AB, Kadhum AAH, Loh KS (2017) Effect of silica on the thermal behavior and ionic conductivity of mixed salt solid acid composites. J Alloys Compd 690:896–902. https://doi.org/10.1016/j.jallcom.2016.08.188
23. JCPDS File of CsH_2PO_4 card No. 84–0122, Joint Committee on Powder Diffraction Standards.
24. JCPDS File of ZrO_2 card No. 37–1484, Joint Committee on Powder Diffraction Standards.
25. Ponomareva VG, Shutova ES, Lavrova GV (2008) Electrical conductivity and thermal stability of (1–x) CsH2PO4/xSiPyOz (x = 0.2–0.7). Compos Inorgan Mater 44:1009–1014
26. Bagryantseva IN, Ponomarevaa VG, Lazarevaa NP (2019) Proton-conductive membranes based on CsH_2PO_4 and ultra-dispersed polytetra fluoroethylene. Solid State Ionics 32:61–66
27. Muroyama H, Matsui T, Kikuchi R, Eguchi K (2006) Composite effect on the structure and proton conductivity for $CsHSO_4$ electrolytes at intermediate temperatures. J Electrochem Soc 153:A1077. https://doi.org/10.1149/1.2189987
28. Leal JH, Martinez H, Martinez I, Price AD, Goos AG, Botez CE (2018) Stability of the superprotonic conduction of (1–x) CsH2PO4/xSiO2 ($0 \le x \le 0.3$) composites under dry and humid environments. Mater Today Commun 15:11–17. https://doi.org/10.1016/j.mtcomm.2018.02.021
29. Anfimova T, Jensen AH, Christensen E, Jensen JO, Bjerrum NJ, Li Q (2015) CsH_2PO_4/$NdPO_4$ composites as proton-conducting electrolytes for intermediate temperature fuel cells. J Electrochem Soc 162:F436–F441. https://doi.org/10.1149/2.0671504jes
30. Ponomareva VG, Bagryantseva IN (2019) The influence of CsH_2PO_4·H_2O impurity on the proton conductivity and thermal properties of CsH_2PO_4. Solid State Ionics 329:90–94. https://doi.org/10.1016/j.ssi.2018.11.021
31. Metcalfe B, Clark JB (1978) Differential scanning calorimetry of CsH_2PO_4. Thermochim Acta 24:149–153
32. Otomo J, Minagawa N, Wen CJ, Eguchi K, Takahashi H (2003) Protonic conduction of CsH_2PO_4 and its composite with silica in dry humid. Solid State Ionics 156:357–369
33. Chen S, Yin Y, Wang D, Liu Y, Wang X (2005) Structures, growth modes and Spectroscopic properties of small Zirconia clusters. J Cryst Growth 282:498–505
34. Hao Y, Li J, Yang X, Wang X, Lu L (2004) Preparation of ZrO_2–Al_2O_3 composite membranes by Sol-gel. Mater Sci Eng, A 367:243–247
35. Bocchetta P, Ferraro R, Quarto FD (2009) Advances in anodic alumina membranes thin film fuel cell: CsH_2PO_4 pore-filler as proton conductor at room temperature. J Power Sources 187:49–56. https://doi.org/10.1016/j.jpowsour.2008.10.088
36. Rajeh A, Ragab HM, Abutalib MM (2020) Co doped ZnO reinforced PEMA/PMMA composite: structural, thermal, dielectric and electrical properties for electrochemical applications. J Mol Struct 1217:128447. https://doi.org/10.1016/j.molstruc.2020.128447